INORGANIC CHEMISTRY
FRONTIERS

RESEARCH ARTICLE

View Article Online
View Journal | View Issue

Check for updates

Cite this: *Inorg. Chem. Front.*, 2024, **11**, 470

Highly effective synthesis of mercapto-functionalized cubic silsesquioxanes as the first step in designing advanced nano-delivery systems†

Kamil Hanek, Monika Wałęsa-Chorab and Patrycja Żak *

A straightforward protocol for the efficient synthesis of sulfur-substituted silsesquioxanes (SQ), based on the α-hydrothiolation of terminal alkynes and catalyzed by a supersteric NHC–rhodium complex, is presented for the first time. The proposed strategy led to a novel class of nanomaterials with many potential medicinal and synthetic applications which had previously been inaccessible by other methods. As a result, twelve new mercapto-modified SQ derivatives were obtained with yields in the range from 84% to 92% and comprehensively characterized by spectroscopic methods.

Received 12th September 2023,
Accepted 30th October 2023

DOI: 10.1039/d3qi01838e

rsc.li/frontiers-inorganic

Open Access Article. Published on 29 November 2023. Downloaded on 6/5/2026 9:20:13 PM.
This article is licensed under a Creative Commons Attribution 3.0 Unported Licence.

Introduction

Sulfur is one of the most abundant heteroatoms in biological structures and its important advantage is a large number of oxidation states that promote fundamental biological reactions and redox biochemistry. It is present in many compounds which constitute important scaffoldings for drugs in contemporary medicine, providing antibacterial, antiviral, antiallergic and antimalarial properties.[1,2] Among the organic sulfur derivatives, thioesters play a particularly important role, especially in biological systems.[3] Recently, their anticancer properties and cytotoxicity against several cells with a disturbed division cycle have been studied.[4] What is worth mentioning is that thioethers containing catechol groups also exhibit antioxidative properties,[5] so they can protect molecules of DNA and lipids from different radical species. Unfortunately, many drugs with potentially good therapeutic effects are still disregarded due to the lack of bioavailability in clinical trials. Therefore, the development of efficient drug delivery platforms to specific target sites in a controlled manner is critical for the implementation of current advances in diverse areas of medicine.

In the last few decades, much interest has been paid to nanodrug delivery systems which offer multiple benefits in treating chronic human diseases. They could be used as delivery agents, either by encapsulating drugs or through binding to therapeutic agents, and could deliver them to target tissues more precisely and with a controlled release.[6] Although there are several nanocarriers with different drug release profiles, much effort has been devoted to the improvement of the specificity of the nanostructures to target particular tissues in the organism[7] and to reduce immunogenicity, through their chemical functionalization with polymers,[8] natural polysaccharides,[9] antibodies,[10] cell membranes,[11] peptides[12] and tunable surfactants[13] (Scheme 1).

From this point of view, polyhedral oligomeric silsesquioxanes (SQ), which exhibit a variety of attributes that make them attractive as drug delivery agents, have drawn particular attention.[14] Because of their nanoscale size and high charge density, SQ units are easily transferrable through vascular pores, which considerably improves their tissue uptake. Unlike traditional organic compounds, SQ derivatives are colorless, nonvolatile, odorless, non-toxic and can be easily functionalized through the introduction of reactive organic groups to the vertex positions *via* various chemical methods. After suitable modifications, the SQ units gain water-solubility which allows the SQ-based drug delivery systems to be taken orally. Additionally, they can be successfully used as functional group

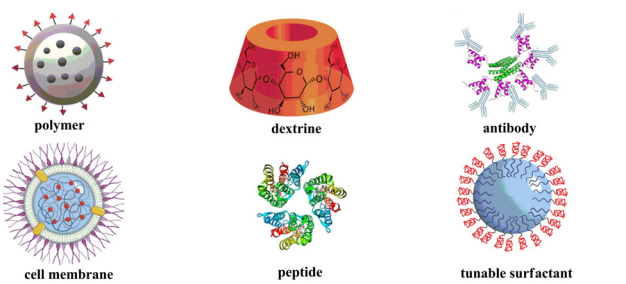

Scheme 1 Nanostructures commonly used as drug delivery systems.

Department of Organometallic Chemistry, Faculty of Chemistry, Adam Mickiewicz University in Poznan, Uniwersytetu Poznańskiego 8, 61-614 Poznan, Poland.
E-mail: pkw@amu.edu.pl

† Electronic supplementary information (ESI) available. See DOI: https://doi.org/10.1039/d3qi01838e

This journal is © the Partner Organisations 2024

Open Access Article. Published on 29 November 2023. Downloaded on 6/5/2026 9:20:13 PM.
This article is licensed under a Creative Commons Attribution 3.0 Unported Licence.

carriers in photodynamic therapy and bioimaging.[15] Their great advantage is also their high thermal stability,[16] simple synthesis and well-defined 3D structure, eliminating issues that arise from the polydispersity of linear polymers. Despite many benefits of SQ-based materials and extensive knowledge in the field of their biomedical application, there is a limited number of reports on their use as nanocarriers. In 2005, Rotello *et al.* described the first controlled drug delivery platform based on SQ scaffolds, which exhibited very low toxicity and enabled the delivery of medicaments that were insoluble in water or exhibited low cellular uptake.[17] The study by Kaneshiro and Lu has shown that the compact and three-dimensional structure of octa(3-aminopropyl)-silsesquioxane-based poly(L-lysine) nanoglobules makes them promising carriers for the codelivery of nucleic acids and chemotherapeutic agents.[18] In 2011, Lin *et al.* reported that polysilsesquioxane (PSQ) nanoparticles are an attractive platform for the delivery of an oxaliplatin prodrug.[19] Four years later, the same group modified the designed material with polyethylene glycol (PEG) and proved its therapeutic potential using the mouse model of non-small cell lung cancer.[20] Application of SQ units as nanocarriers has been explored by Gu and co-workers, who demonstrated that star-shaped poly(benzyl L-aspartate)-*block*-poly (ethylene glycol) copolymers with a POSS core constitute potential carriers for drug delivery.[21] In 2016, Huang *et al.* synthesized SQ-based star polymer–drug conjugates, which were chemically loaded with DTX *via* a pH-responsive linker and demonstrated their *in vitro* applications using a PC-3 human prostate carcinoma cell line.[22] John's team has shown that amido-functionalized cage-like silsesquioxanes can serve as efficient delivery systems of drugs such as acetaminophen and ibuprofen. What is more, they proved that in this system, the adsorbed drug molecules can be released under physiological conditions, and then the SQ-based carrier is able to hydrolyze to non-toxic carboxylic acid salts and water soluble polyhedral oligomeric silsesquioxanes containing aminopropyl groups; thus, the products can be safely removed from the organism.[23] In turn, Sierant's group has developed a multifunctional nanoplatform based on inorganic SQ grafted with short polyethylene glycol chains and anthracycline antibiotics called daunorubicin.[24] Two years later, Stanczyk *et al.* confirmed that SQ nanocarriers are useful systems for the formation of conjugates with anthracycline drugs.[25] Recently, it has been proved that the incorporation of SQ with thiol groups into the drug can increase its efficiency in photothermal activity in the treatment of pancreatic cancer.[26] To the best of our knowledge, this is the only known example of application of the drug functionalized with an SQ-SH carrier, in which the carrier not only creates the delivery system but also improves the therapeutic potential of the drug itself.

In view of the high demand for modern drug delivery platforms and continuous search for carrier molecules that would contribute to the improvement of the therapeutic properties of the drugs, new SQ-SH functionalized nanocarriers that would be readily adjusted to specific needs by further modifications are highly desirable. Herein, we describe an effective synthetic pathway for obtaining a new class of functionalized SQ derivatives containing thioester moieties, *via* reactions of mercapto-SQ (**SQ-SH**) and alkynes, in the presence of a bulky NHC–rhodium complex. The final materials, providing a universal platform for developing non-toxic and effective drugs, are obtained in a straightforward, one-step procedure based on commercially available reagents.

Results and discussion

Catalytic part

We began our research with the synthesis of a rhodium catalyst containing a bulky NHC ligand (**NHC-Rh**), according to the methodology described in our previous paper[27] (Scheme 2).

Because of the lack of literature reports on the use of mercapto-SQ as substrate in the hydrothiolation process, we started our catalytic study by performing a number of tests under the same conditions as those described for other thiols in our previous work.[27] Addition of 1 mol% **NHC-Rh** to a toluene solution of **SQ-SH** and phenylacetylene (**1a**) in an equimolar ratio at 80 °C, resulted in 50% conversion of substrates after 24 h (Scheme 3).

As the ^{1}H NMR analysis of the reaction mixture indicated selective formation of a single product, identified as **P1**, we decided to optimize the reaction conditions in order to shift the process equilibrium towards the expected product. All experiments were performed for the model reaction shown in Scheme 3. The results are given in Table 1.

As presented in Table 1, a two-fold increase in the catalyst concentration did not bring the expected effect as the degree of **SQ-SH** conversion increased only by 9% (Table 1, entry 2). It has been found that temperature was the factor significantly influencing the effectiveness of the reaction studied. With increasing temperature, the degree of the reagent conversion increased (Table 1, entries 2–5) to reach 100% at 120 °C (Table 1, entry 5). Importantly, the temperature increase had no effect on the process selectivity, as at each temperature only α-vinyl sulfides were obtained. When the catalyst loading was lower than 2 mol%, complete conversion of **SQ-SH** was not achieved, even though the reaction time was much increased (Table 1, entry 8). As shown in Table 1, we discovered that the reaction must be carried out under dry argon, using standard Schlenk-line and vacuum techniques (Table 1, entry 9) and necessarily in the presence of the catalyst (Table 1, entry 10). In the tests conducted under dry argon, we observed the for-

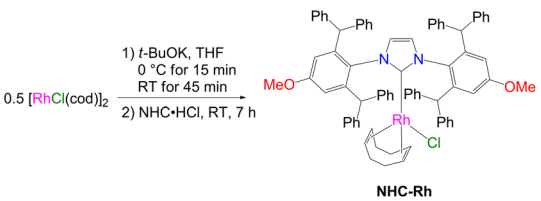

Scheme 2 Synthesis of the NHC–rhodium catalyst (**NHC-Rh**).

Open Access Article. Published on 29 November 2023. Downloaded on 6/5/2026 9:20:13 PM.
This article is licensed under a Creative Commons Attribution 3.0 Unported Licence.

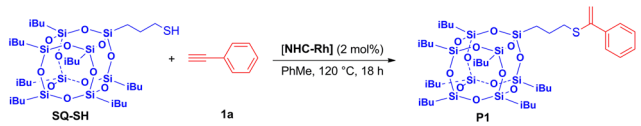

Scheme 3 Hydrothiolation of **1a** with **SQ-SH** catalyzed by **NHC-Rh**.

Table 1 Optimization of reaction conditions

Entry	[NHC-Rh] [mol%]	*T* [°C]	Conv. of SQ-SH[c] [%]	Selectivity[c] [%]
1	1	80	50	100
2	2	80	59	100
3	2	100	78	100
4	2	110	88	100
5	**2**	**120**	**100**	**100**
6	1.5	120	94	100
7	1	120	90	100
8[a]	1	120	92	100
9[b]	2	120	70	12
10	—	120	0	—

Reaction conditions: toluene, [**SQ-SH**] : [**1a**] = 1 : 1, 18 h, and argon. [a] Time reaction: 48 h. [b] Reaction conducted under air. [c] Determined by ^{1}H NMR analysis.

mation of significant amounts of disulfides and trace amounts of product **P10**. The results suggest that the formation of the S–S bond requires tan excess of oxygen as then this process is favored over that of C–S formation. It is in agreement with the mechanism of this process described earlier by Arisawa's group[28] and our earlier paper.[29]

Subsequently, the range of alkynes was extended to determine the versatility of this catalytic protocol (Scheme 4).

In the experiments performed under optimized conditions, no competitive reactions were noted. For all acetylenes tested, high yields and exclusive formation of the expected products were observed. We did not note any impact of the nature of the alkyne used on the reaction course, except in the experiment conducted using out dimethylsilylacetylene. In this case, we obtained as the product the β-isomer of *E* geometry around the generated C=C double bond (**P11**). The proposed method proved to be effective for aryl substituted alkynes with both electron-withdrawing and electron-donating substituents. As presented in Scheme 4, dialkyne was also applied in the reaction with **SQ-SH** and exhibited high activity leading to a monosubstituted product (**P12**). This opens up the possibility of synthesizing materials that may contain groups susceptible to further modification. All functionalized SQ derivatives obtained were characterized by mass spectrometry and spectroscopic methods (see the ESI†). They are air-stable and soluble in many popular solvents (*i.e.*, DCM, THF, *n*-hexane, toluene and chloroform), which makes them easy to purify by column chromatography. The presented derivatives are new compounds which have never been published before.

Photophysical properties

In the next step, the prepared nanomaterials (**P1–P12**) were subjected to photophysical analyses, which were performed to investigate their potential applications in the optical area. At first the absorption spectra in the ultraviolet/visible (UV-Vis) region were recorded. The absorption properties were investigated in chloroform solutions and the appropriate spectra are shown in Fig. 1.

The absorption spectra of all compounds except for **P12** show the onset of absorption at around 400 nm. The more pronounced absorption was observed in the medium- and short-wave ultraviolet range with the absorption maxima in the range of 240–300 nm, depending on the substituent. The absorption maximum of the styrene derivative **P1** was located at 245 nm. It was observed that the electron-withdrawing substituents (–CF_3) at the phenyl ring caused a slight blue shift whereas the electron-donating substituents (alkyl substituents) caused a slight red shift. Although the 1-ethynyl group is considered an electron withdrawing substituent,[30] the greatest bathochromic shift (by 16 nm) was observed for the 1-ethynyl derivative **P11**, because of an increase in conjugation.[31] For the naphthalene derivative **P9**, three absorption peaks were observed, at 274 nm, 285 nm and 297 nm, characteristic of naphthalene and its derivatives.[32] For all compounds except for **P9** and **P12**, a shoulder of weak absorption intensity appeared in the range from 400 nm to 300 nm.

The photoluminescent behavior of all compounds was also investigated in chloroform solutions. For the naphthalene derivative **P9**, the structured narrow emission characteristic of naphthalene derivatives was noted (see the ESI, Fig. S1†). Samples **P1–P7** and **P10**, when excited at the respective absorption maxima exhibited weak emission in the UV region with the emission maxima in the range 340–380 nm, due to the local emission of the styrene fluorophore (see the ESI, Fig. S2†).[33] Similarly, the thiophene derivative **P8** exhibited weak emission in the UV range, while the silyl derivative **P12** was found to be almost non-emissive. Compound **P11** exhibited weak emission in the blue region with the emission maximum at 450 nm. The emission peak was very broad and spread up to 600 nm. The emission was found to be enhanced for compounds **P5** and **P6**, containing electron withdrawing CF_3 groups (see the ESI, Fig. S3†). The dependence of the photoluminescence on the excitation wavelength in the range from 250 to 380 nm was investigated (Fig. 2 and in the ESI, Fig. S4–S12†) and strong changes in the emission intensity and the shape of the emission spectra for samples **P1–P4**, **P7** and **P10–P11** were discovered.

These changes were not observed for the naphthalene derivative **P9**, thiophene derivative **P8** and CF_3 derivatives **P5** and **P6**. Therefore, we carried out an analysis of the excitation spectra and we found that there was another notable area of excitation at a lower energy, between 300 nm and 380 nm (Fig. 3).

The excitation and absorption spectra of the investigated compounds were found to be different. The obtained results indicate that the samples do not obey the Kasha's rule.[34] The peak of lower energy dominates in the excitation spectra of the

 This journal is © the Partner Organisations 2024

Open Access Article. Published on 29 November 2023. Downloaded on 6/5/2026 9:20:13 PM.
This article is licensed under a Creative Commons Attribution 3.0 Unported Licence.

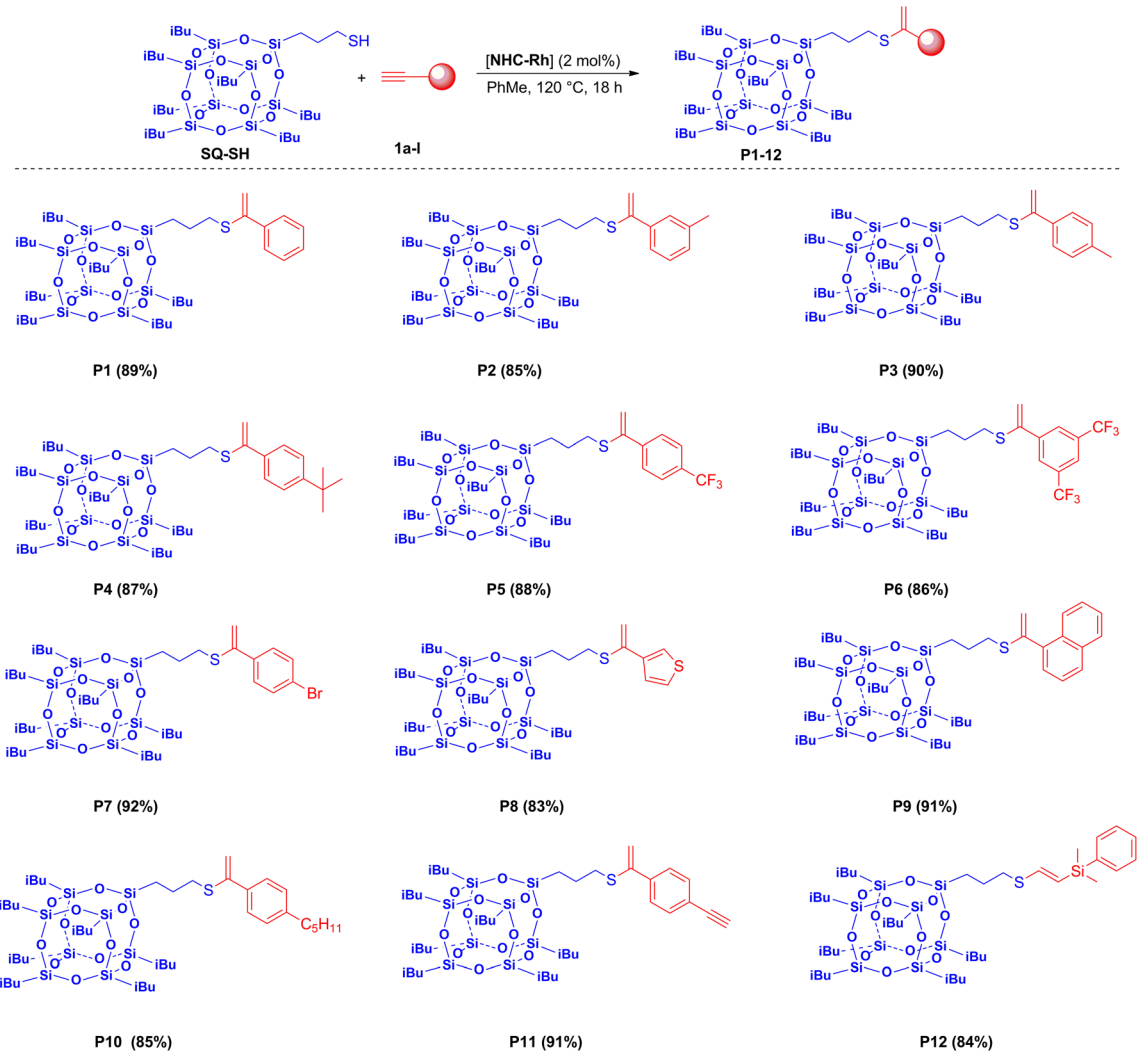

Scheme 4 Substrate scope. Isolated yields are given in parentheses.

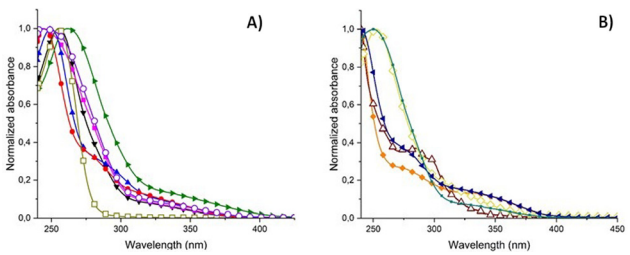

Fig. 1 Normalized absorption spectra of compounds (A): **P1** (●), **P2** (▲), **P3** (■), **P4** (▼), **P10** (○), **P11** (▶), **P12** (□); (B): **P5** (◀), **P6** (♦), **P7** (▬), **P8** (◊), **P9** (Δ).

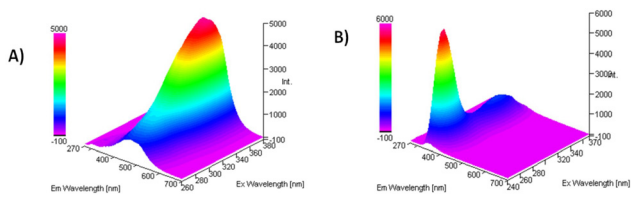

Fig. 2 The dependence of photoluminescence on the excitation wavelength for compounds (A): **P11** and (B) **P6**.

styrene derivative **P1**, compounds containing electron-donating alkyl substituents, bromine derivative **P7** and 1-ethynyl derivative **P11**. We further investigated the emission properties after excitation at the lower energy excitation maxima (Fig. 4).

The summarized spectroscopic data are presented in Table 2.

Compounds **P1–P4** and **P10** containing styrene or styrene with alkyl substituents, exhibited emission in the UV range. The emission maxima were located at around 400 nm and they were red shifted in comparison with the emission observed after excitation at the absorption maxima. This suggests that this longer-wavelength emission can be attributed to the styrene excimer emission.[35] It was observed that incorporation of the alkyl did not significantly influence the emission intensity. The most interesting emission properties were observed for the 1-ethynyl derivative **P11**. The compound after excitation at 364 nm exhibited strong

Open Access Article. Published on 29 November 2023. Downloaded on 6/5/2026 9:20:13 PM.
This article is licensed under a Creative Commons Attribution 3.0 Unported Licence.

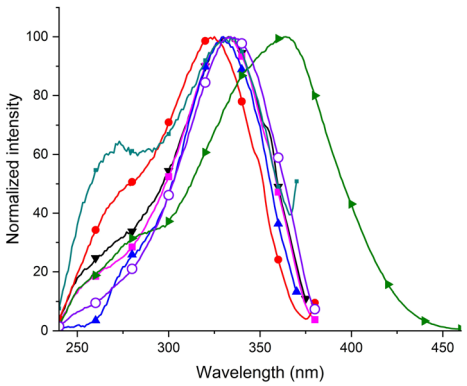

Fig. 3 Excitation spectra of compounds **P1** (●) (λ_{em} = 391 nm), **P2** (▲) (λ_{em} = 401 nm), **P3** (■) (λ_{em} = 399 nm), **P4** (▼) (λ_{em} = 399 nm), **P7** (■) (λ_{em} = 396 nm), **P10** (○) (λ_{em} = 401 nm) and **P11** (▶) (λ_{em} = 502 nm).

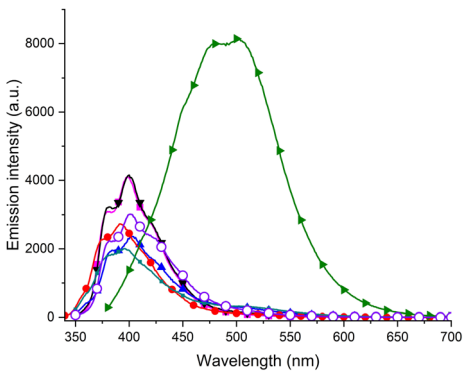

Fig. 4 The emission spectra of compounds **P1** (●) (λ_{ex} = 325 nm), **P2** (▲) (λ_{ex} = 330 nm), **P3** (■) (λ_{ex} = 330 nm), **P4** (▼) (λ_{ex} = 333 nm), **P7** (■) (λ_{ex} = 334 nm), **P10** (○) (λ_{ex} = 334 nm) and **P11** (▶) (λ_{ex} = 364 nm).

Table 2 Spectroscopic data of compounds **P1–P12**

Compound	$\lambda_{abs.}$ [nm]	λ_{ex} [nm]	λ_{em} [nm]
P1	245	325	391[a]
P2	250	330	401[a]
P3	245	330	399[a]
P4	255	333	399[a]
P5	242	—	348[b]
P6	242	—	348[b]
P7	250	334	396[a]
P8	252	—	340[a]
P9	274, 285, 297	—	355, 372, 390[c]
P10	245	334	401[a]
P11	261	364	478, 502[a]
P12	255	—	—

[a] Excited at excitation maxima. [b] Excited at absorption maxima. [c] Excited at absorption maxima λ = 285 nm.

luminescence in the visible range with two emission maxima at 478 nm and 502 nm and the emitted light of blue color was visible by naked eye after irradiation with a UV lamp (Fig. 5). The *xy* color coordinates of the light emitted by compound **P11** were calculated and found to be (0.28; 0.11).

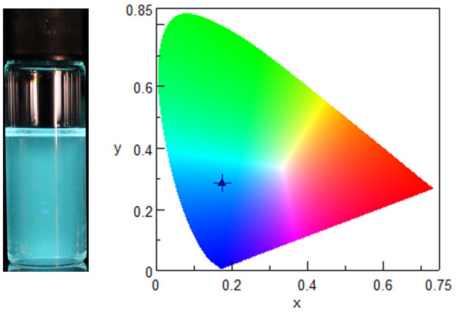

Fig. 5 Left: the photograph of the compound **P11** in $CHCl_3$ solution when excited using a UV lamp (λ = 365 nm); right: CIE chromaticity diagram showing the (*x*,*y*) emission color coordinates for the **P11**.

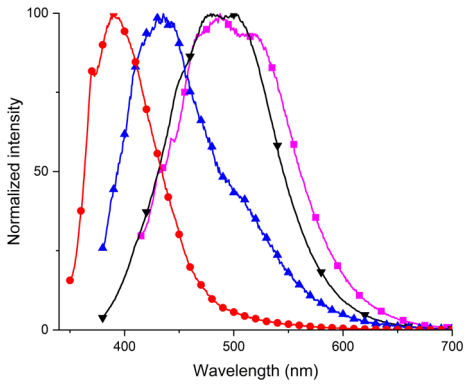

Fig. 6 The emission spectra of compound **P11** in solvents of different polarities: *n*-hexane (●) (λ_{ex} = 337 nm), ethyl acetate (▲) (λ_{ex} = 364 nm), acetonitrile (■) (λ_{ex} = 380 nm), chloroform (▼) (λ_{ex} = 364 nm).

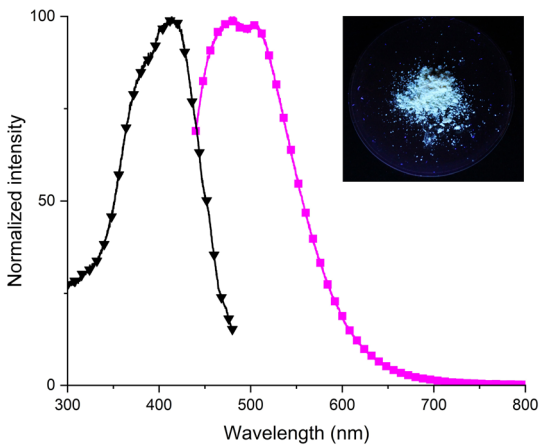

Fig. 7 The excitation (▼) (λ_{em} = 504 nm) and emission spectra (■) (λ_{ex} = 413 nm) of **P11** in the solid state. Insert: photograph showing the emission of **P11** in the solid state when excited using a UV lamp (λ = 365 nm).

The emission properties of **P11** were further investigated in *n*-hexane, ethyl acetate and acetonitrile. These solvents have been chosen due to their different polarities and ability to solubilize **P11**. The shift of the emission maxima to

This journal is © the Partner Organisations 2024

Open Access Article. Published on 29 November 2023. Downloaded on 6/5/2026 9:20:13 PM. This article is licensed under a Creative Commons Attribution 3.0 Unported Licence.

longer wavelengths was observed with the increase in solvent polarity (from 391 nm in *n*-hexane to 518 nm in acetonitrile) (Fig. 6).

The compound was also luminescent in the solid state. When excited at excitation maxima (λ_{ex} = 413 nm), the solid exhibited blue emission with two maxima at 480 nm and 504 nm (Fig. 7).

Conclusions

To sum up, we have designed a fully selective and high yield synthetic procedure, which allows obtaining new sulfur-containing SQ derivatives. We have demonstrated that the proposed approach can be easily extended to a variety of other commonly available alkynes, which offers a high chance of using the designed materials as non-toxic nanocarriers that would additionally contribute to the improvement of the therapeutic properties of drugs. Finally, twelve new sulfur-based SQs were obtained and characterized by NMR spectroscopy and mass spectrometry. They were also verified in terms of their absorption and emission properties. We have shown that these materials are luminescent with the maximum emission in the ultraviolet range. The most interesting luminescence properties were exhibited by a 1-ethynyl derivative which showed bright blue fluorescence under 365 nm UV lamp illumination; therefore, it could be potentially applied as a blue light-emitting material. It is particularly interesting in the context of literature reports indicating the use of blue light in cancer therapy.[36]

Experimental

General consideration

Reagents. All reagents, except NHC carbene precursors and the NHC–rhodium complex, were commercially available and used as received. NHC salt[37] and the rhodium catalyst[27] were prepared according to literature procedures. All syntheses were carried out under an argon atmosphere using standard Schlenk-line and vacuum techniques. THF was dried over sodium benzophenone ketyl and freshly distilled before use. The other solvents were dried over CaH_2 prior to use and stored over 4 Å molecular sieves under argon. Dichloromethane was additionally passed through an alumina column and degassed by repeated freeze–pump–thaw cycles.

Instruments and measurements

Nuclear magnetic resonance (NMR) spectroscopy. ^{1}H NMR (402.6 MHz), ^{13}C NMR (101.2 MHz) and ^{29}Si NMR (79 MHz) spectra were recorded at 25 °C on Varian 400 and 300 MHz spectrometers in $CDCl_3$ solution. Chemical shifts are reported in ppm with reference to the residual solvent peaks for ^{1}H and ^{13}C NMR and to TMS for ^{29}Si NMR.

Electrospray ionization mass spectrometry (ESI-MS). Mass spectra were obtained using Synapt Gs-S HDMS (Waters) mass spectrometer with an electrospray ion source and quadrupole-time-of-flight analyzer with resolving power FWMH 38000. Acetonitrile was used as the sample solvent. The capillary voltage was set to 4.5 kV, the sampling was set at 40 and the source temperature was equal to 120 °C. The most abundant ions in the ESI-MS spectra were the sodiated and potassiated ions of desired products.

Thin-layer chromatography (TLC). TLC was conducted on plates coated with 250 μm thick silica gel and column chromatography was performed on silica gel 60 (70–230 mesh) using *n*-hexane.

Photophysical analyses. Absorption spectra were recorded on a Jasco V-770 UV-Vis-NIR spectrometer (Fig. 1). Fluorescence measurements were performed and excitation spectra collected at room temperature in chloroform solutions with a Jasco FP-8500 spectrometer. The excitation and emission slits were 5 nm for excitation at the absorption maxima (spectra shown in Fig. S1–S3†) and 2.5 nm for excitation at excitation maxima (spectra shown in Fig. 3). The absorption of the solutions of the compounds for fluorescence measurements was around 0.1 at the excitation wavelength. The samples were purged with argon for 15 minutes. The emission and excitation spectra of **P11** in the solid state were recorded using an integrating sphere (100 mm) that had been calibrated using a calibrated light source.

General procedure for the synthesis of products P1–P12

An oven-dried 25 mL glass reactor equipped with a magnetic stirring bar was charged under argon with **SQ-SH** (100 mg, 1.12×10^{-4} mol), acetylene (1.12×10^{-4} mol), NHC–rhodium complex (5.60×10^{-6} mol) and toluene (1 mL). The reaction mixture was stirred at 120 °C for 24 hours. The solvent was then evaporated under vacuum and the residue was purified by column chromatography on silica gel using *n*-hexane as the eluent. Evaporation of the solvents afforded analytically pure compounds.

Author contributions

Kamil Hanek: preparation of an NHC precursor and a rhodium complex, performance of synthesis and isolation of all products; Monika Wałęsa-Chorab: optical studies, data analysis, and writing – original draft; Patrycja Żak: conceptualization of the paper, design of the experiments, data analysis, writing original draft and supervision of the research. All authors have read and agreed to the published version of the manuscript.

Conflicts of interest

There are no conflicts to declare.

Open Access Article. Published on 29 November 2023. Downloaded on 6/5/2026 9:20:13 PM.
This article is licensed under a Creative Commons Attribution 3.0 Unported Licence.

Acknowledgements

The authors gratefully acknowledge the financial support from the National Science Centre (Poland) (Project Sonata Bis No. 2019/34/E/ST5/00103).

References

1 M. Fenga, B. Tang, S. H. Liang and X. Jiang, Sulfur Containing Scaffolds in Drugs: Synthesis and Application in Medicinal Chemistry, *Curr. Top. Med. Chem.*, 2016, **16**(11), 1200–1216.
2 H. Guo, B. Sun, H. Gao, X. Chen, S. Liu, X. Yao, X. Liu and Y. Che, Diketopiperazines from the cordyceps-colonizing fungus Epicoccum nigrum, *J. Nat. Prod.*, 2009, **72**(12), 2115–2119.
3 M. Frenkel-Pinter, M. Bouza, F. M. Fernández, L. J. Leman, L. D. Williams, N. V. Hud and A. Guzman-Martinez, Thioesters provide a plausible prebiotic path to proto-peptide, *Nat. Commun.*, 2022, **13**, 2569.
4 M. Ihsan Han and Ş. G. Küçükgüzel, Thioethers: An Overview, *Curr. Drug Targets*, 2022, **23**, 2, DOI: **10.2174/1389450122666210614121237**.
5 I. V. Smolyaninov, D. A. Burmistrova, M. V. Arsenyev, M. A. Polovinkina, N. P. Pomortseva, G. K. Fukin, A. I. Poddel'sky and N. T. Berberova, Synthesis and Antioxidant Activity of New Catechol Thioethers with the Methylene Linker, *Molecules*, 2022, **27**, 3169.
6 J. K. Patra, G. Das, L. F. Fraceto, E. V. R. Campos, M. del Pilar Rodrigues-Torres, L. S. Acosta-Torres, L. A. Diaz-Torres, R. Grillo, M. K. Swamy, S. Sharma, S. Habtemariam and H.-S. Shin, Nano based drug delivery systems: recent developments and future prospects, *J. Nanobiotechnol.*, 2018, **16**, 71.
7 V. P. Torchilin, Multifunctional nanocarriers, *Adv. Drug Delivery Rev.*, 2012, **64**, 302–315.
8 B. Pelaz, P. del Pino, P. Maffre, R. Hartmann, M. Gallego, S. Rivera_Fernandez, J. M. de la Fuente, G. U. Nienhaus and W. J. Parak, Surface functionalization of nanoparticles with polyethylene glycol: effects on protein adsorption and cellular uptake, *ACS Nano*, 2015, **9**(7), 6996–7008.
9 (*a*) A. Almalik, H. Benabdelkamel, A. Masood, I. O. Alanzi, I. Alradwan, M. A. Majrashi, A. A. Alfadda, W. M. Alghamdi, H. Alrabiah, N. Tirelli and A. H. Alhasan, Hyaluronic acid coated chitosan nanoparticles reduced the immunogenicity of the formed protein corona, *Sci. Rep.*, 2017, **7**, 10542; (*b*) T. F. Martens, K. Remaut, H. Deschout, J. F. J. Engbersen, W. E. Hennink, M. J. van Steenbergen, J. Demeester, S. C. Smedt and K. Braeckmans, Coating nanocarriers with hyaluronic acid facilitates intravitreal drug delivery for retinal gene therapy, *J. Controlled Release*, 2015, **202**, 83–92.
10 P. Kolhar, A. C. Anselmo, V. Gupta, K. Pant, B. Prabhakarpandian, E. Ruoslahti and S. Mitragotri, Using shape effects to target antibody-coated nanoparticles to lung and brain endothelium, *Proc. Natl. Acad. Sci. U. S. A.*, 2013, **110**, 10753–10758.
11 W. W. Gao and L. F. Zhang, Coating nanoparticles with cell membranes for targeted drug delivery, *J. Drug Target.*, 2015, **23**, 619–626.
12 H. Gao, Z. Yang, S. Zhang, S. Cao, S. Shen, Z. Pang and X. Jiang, Ligand modified nanoparticles increases cell uptake, alters endocytosis and elevates glioma distribution and internalization, *Sci. Rep.*, 2013, **3**, 2534.
13 J. Muller, K. N. Bauer, D. Prozeller, J. Simon, V. Mailander, F. R. Wurm, S. Winzen and L. Landfester, Coating nanoparticles with tunable surfactants facilitates control over the protein corona, *Biomaterials*, 2017, **115**, 1–8.
14 For review see: (*a*) B. Cordes, P. D. Lickiss and F. Rataboul, Recent developments in the chemistry of cubic polyhedral oligosilsesquioxanes, *Chem. Rev.*, 2010, **110**, 2081–2173; (*b*) F. Dong, L. Lu and C. S. Ha, Silsesquioxane-containing hybrid nanomaterials: fascinating platforms for advanced applications, *Chem. Phys.*, 2019, **220**, 1800324; (*c*) Y. Du and H. Liu, Cage-like Silsesquioxanes-based Hybrid Materials, *Dalton Trans.*, 2020, **49**, 5396–5406.
15 P. Loman-Cortes, T. Binte-Hug and J. L. Vivero-Escoto, Use of Polyhedral Oligomeric Silsesquioxane (POSS) in Drug Delivery, Photodynamic Therapy and Bioimaging, *Molecules*, 2021, **26**(21), 6453.
16 (*a*) L. Li and H. Liu, Rapid Preparation of Silsesquioxane-Based Ionic Liquids, *Chem. – Eur. J.*, 2016, **22**, 4713–4716; (*b*) X. Zhao, Q. Wang, R. Kunthom and H. Liu, Sulfonic Acid-Grafted Hybrid Porous Polymer Based on Double-Decker Silsesquioxane as Highly Efficient Acidic Heterogeneous Catalysts for the Alcoholysis of Styrene Oxide, *ACS Appl. Mater. Interfaces*, 2023, **15**, 6657–6665.
17 C. McCusker, J. B. Carroll and V. M. Rotello, Cationic polyhedral oligomeric silsesquioxane (POSS) units as carriers for drug delivery processes, *Chem. Commun.*, 2005, 996–998.
18 T. L. Kaneshiro and Z.-R. Lu, Targeted intracellular codelivery of chemotherapeutics and nucleic acid with a well-defined dendrimer-based nanoglobular carrier, *Biomaterials*, 2009, **30**, 5660–5666.
19 J. D. Rocca, R. C. Huxford, E. Comstock-Duggan and W. Lin, Polysilsesquioxane Nanoparticles for Targeted Platin-Based Cancer Chemotherapy by Triggered Release, *Angew. Chem., Int. Ed.*, 2011, **50**, 10330–10334.
20 J. D. Rocca, M. E. Werner, S. A. Kramer, R. C. Huxford-Phillips, R. Sukumar, N. D. Cummings, J. L. Vivero-Escoto, A. Z. Wang and W. Lin, Polysilsesquioxane nanoparticles for triggered release of cisplatin and effective cancer chemoradiotherapy, *Nanomedicine*, 2015, **11**(1), 31–38.
21 C. Y. Pu, L. Zhang, H. Zheng, B. He and Z. Gu, Synthesis and Drug Release of Star-Shaped Poly(benzyl L-aspartate)-block-poly(ethylene glycol) Copolymers with POSS, *Macromol. Biosci.*, 2014, **14**, 289–297.
22 Q. Yang, L. Li, W. Li, Z. Zhou and Y. Huang, Dual Stimuli-Responsive Hybrid Polymeric Nanoparticles Self-Assembled from POSS-Based Starlike Copolymer-Drug Conjugates for

 This journal is © the Partner Organisations 2024

Open Access Article. Published on 29 November 2023. Downloaded on 6/5/2026 9:20:13 PM.
This article is licensed under a Creative Commons Attribution 3.0 Unported Licence.

Efficient Intracellular Delivery of Hydrophobic Drugs, *ACS Appl. Mater. Interfaces*, 2016, **8**(21), 13251–13261.

23 Ł. John, M. Malik, M. Janeta and S. Szafert, First step towards a model system of the drug delivery network based on amide-POSS nanocarriers, *RSC Adv.*, 2017, **7**, 8394–8401.

24 K. Rózga-Wijas and M. Sierant, Daunorubicin-silsesquioxane conjugates (POSS-DAU) for theranostic drug delivery system: Characterization, biocompatibility and drug release study, *React. Funct. Polym.*, 2019, **143**, 104332.

25 K. Piorecka, J. Jurjata and W. A. Stanczyk, Novel Polyhedral Silsesquioxanes [POSS(OH)32] as Anthracycline Nanocarriers – Potential Anticancer Prodrugs, *Molecules*, 2021, **26**, 47.

26 S. Abudukelimu, G. Wei, J. Huang, G. Zhao, L. Wei, W. Cui, M. Lu and W. Yao, Polyhedral oligomeric silsesquioxane (POSS)-based hybrid nanocomposite for synergistic chemo-photothermal therapy against pancreatic cancer, *J. Chem. Eng.*, 2022, 136124.

27 M. Bołt, L. Delaude and P. Żak, Rhodium catalysts with superbulky NHC ligands for the selective α-hydrothiolation of alkynes, *Dalton Trans.*, 2022, **51**, 4429–4434.

28 M. Arisawa, K. Fukumoto and M. Yamaguchi, Rhodium-Catalyzed Oxidation of Unprotected Peptide Thiols to Disulfides with Oxygen in Water, *ACS Catal.*, 2020, **10**, 15060–15064.

29 M. Bołt and P. Żak, Application of Bulky NHC−Rhodium Complexes in Efficient S−Si and S−S Bond Forming Reactions, *Inorg. Chem.*, 2021, **60**, 17579–17585.

30 X. Lucas, D. Quiñonero, A. Frontera and P. M. Deyà, Counterintuitive Substituent Effect of the Ethynyl Group in Ion−π Interactions, *J. Phys. Chem. A*, 2009, **113**, 10367–10375.

31 H.-H. Park, P. Meti and Y.-D. Gong, Effect of conjugation on the optoelectronic properties of pyrazine-based push-pull chromophores: Aggregation-induced emission, solvatochromism, and acidochromism, *Dyes Pigm.*, 2021, **190**, 109320.

32 H. Maeda, T. Maeda and K. Mizuno, Absorption and Fluorescence Spectroscopic Properties of 1- and 1,4-Silyl-Substituted Naphthalene Derivatives, *Molecules*, 2012, **17**, 5108–5125.

33 A. Ferrer-Ugalde, E. J. Juárez-Pérez, F. Teixidor, C. Viñas and R. Núñez, Synthesis, characterization, and thermal behavior of carboranyl-styrene decorated octasilsesquioxanes: Influence of the carborane clusters on photoluminescence, *Chem. – Eur. J.*, 2013, **19**, 17021–17030.

34 A. P. Demchenko, V. I. Tomin and P.-T. Chou, Breaking the Kasha Rule for More Efficient Photochemistry, *Chem. Rev.*, 2017, **117**, 13353–13381.

35 C. Qu, Z. Li and J. He, Synthesis of copolymers with an exact alternating sequence using the cationic polymerization of pre-sequenced monomers, *Polym. Chem.*, 2018, **9**, 3455–3460.

36 (*a*) B. S. Swami Vetha, P.-S. Oh, S. H. Kim and H.-J. Jeong, Curcuminoids encapsulated liposome nanoparticles as a blue light emitting diode induced photodynamic therapeutic system for cancer treatment, *J. Photochem. Photobiol., B*, 2020, **205**, 111840; (*b*) T. Yoshimoto, M. Shimada, T. Tokunaga, T. Nakao, M. Nishi, Ch. Takasu, H. Kashihara, Y. Wada, S. Okikawa and K. Yoshikawa, Blue light irradiation inhibits the growth of colon cancer and activation of cancer-associated fibroblasts, *Oncol. Rep.*, 2022, **47**(5), 104.

37 M. Hans, J. Lorkowski, A. Demonceau and L. Delaude, Efficient synthetic protocols for the preparation of common N-heterocyclic carbene precursors, *Beilstein J. Org. Chem.*, 2015, **11**, 2318–2325.